WOODS HOLE OCEANOGRAPHIC INSTITUTION

Applied Ocean Physics and Engineering Department

March 30, 2016

Dr. Kyle Becker
Office of Naval Research, Code 322
One Liberty Center
875 North Randolph Street
Arlington, VA 22203-1995

Dear Dr. Becker:

Enclosed is the Final Report for ONR Grant No. N00014-13-1-0026 entitled "Three-Dimensional Shallow Water Acoustics," Principal Investigator Dr. Ying-Tsong Lin.

Sincerely,

Gretchen McManamin

Gretchen McManamin
Administrative Assistant to Dr. Ying-Tsong Lin

Enclosure

cc: Administrative Grants Officer
Defense Technical Information Office
Naval Research Laboratory
Grant and Contract Services (WHOI)
AOPE Department Office (WHOI)

MS#12 • Woods Hole, MA 02543 USA • 508.289.2230 • Fax 508.457.2194

REPORT DOCUMENTATION PAGE

Form Approved
OMB No. 0704-0188

1. REPORT DATE *(DD-MM-YYYY)*	2. REPORT TYPE	3. DATES COVERED *(From – To)*
30/03/2016	FINAL	01/01/2013-12/31/2015

4. TITLE AND SUBTITLE

Three-Dimensional Shallow Water Acoustics

5a. CONTRACT NUMBERS

5b. GRANT NUMBER

N00014-13-1-0026

5c. PROGRAM ELEMENT NUMBER

6. AUTHOR(S)

Dr. Ying Tsong Lin

5d. PROJECT NUMBER

WHOI Project No. 13002600

5e. TASK NUMBER

5f. WORK UNIT NUMBER

7. PERFORMING ORGANIZATION NAME(S) AND ADDRESS(ES)

Woods Hole Oceanographic Institution
266 Woods Hole Road
Woods Hole, MA 02543

8. PERFORMING ORGANIZATION REPORT NUMBER

9. SPONSORING/MONITORING AGENCY NAME(S) AND ADDRESS(ES)

Dr. Kyle Becker
Office of Naval Research
One Liberty Center, Code 322
875 North Randolph Street
Arlington, VA 22203-1995

10. SPONSORING/MONITORING ACRONYM(S)

ONR

11. SPONSORING/MONITORING AGENCY REPORT NUMBER

12. DISTRIBUTION/AVAILABILITY STATEMENT

Approved for public release; distribution is unlimited

13. SUPPLEMENTARY NOTES

14. ABSTRACT

Both physical oceanographic processes and marine geological features in the areas of continental shelf and shelfbreak can cause horizontal heterogeneity in medium properties, so horizontal refraction and reflection of sound can occur and produce significant three-dimensional (3-D) sound propagation effects. The long-term goals of this project are targeted on understanding the 3-D acoustic effects, and their temporal and spatial variability, caused by the environmental factors existing commonly in the continental shelf and shelfbreak areas, such as slopes, submarine canyons, sub-bottom layers, surface waves, internal waves and shelfbreak fronts.

15. SUBJECT TERMS

Continental Shelf; 3-D Acoustics, Surface Waves, Sound Propagation

16. SECURITY CLASSIFICATION OF:			17. LIMITATION OF ABSTRACT	18. NUMBER OF PAGES	19a. NAME OF RESPONSIBLE PERSON
a. REPORT	b. ABSTRACT	c. THIS PAGE	None	24	Ying Tsong Lin
Unclassified	Unclassified	Unclassified			19 b. TELEPHONE NUMBER *(Include are code)* 508-289-2329

Final Report

Three-Dimensional Shallow Water Acoustics

Dr. Ying-Tsong Lin
Applied Ocean Physics and Engineering Department
Woods Hole Oceanographic Institution, Woods Hole, MA 02543
phone: (508) 289-2329 fax: (508) 457-2194 email: ytlin@whoi.edu

Award Number: N00014-13-1-0026

LONG-TERM GOALS

Both physical oceanographic processes and marine geological features in the areas of continental shelf and shelfbreak can cause horizontal heterogeneity in medium properties, so horizontal refraction and reflection of sound can occur and produce significant three-dimensional (3-D) sound propagation effects. The long-term goals of this project are targeted on understanding the 3-D acoustic effects, and their temporal and spatial variability, caused by the environmental factors existing commonly in the continental shelf and shelfbreak areas, such as slopes, submarine canyons, sub-bottom layers, surface waves, internal waves and shelfbreak fronts.

OBJECTIVES

A verity of physical oceanographic processes and marine geological features can cause lateral inhomogeneity of the medium properties in the ocean. Thus, horizontal refraction and reflection of sound can occur and produce significant 3-D acoustic propagation effects. One of the research objectives in this project is to develop efficient and accurate models (both theoretical and numerical models) for studying underwater sound propagation in complex ocean environments. The ultimate scientific objective is to study the underlying physics of the 3D sound propagation effects caused jointly by physical oceanographic processes and geological features. To achieve this goal, individual environmental factor will be first studied and then considered jointly with a unified ocean, seabed and acoustic model. Another major objective is to develop a tangent linear model to predict acoustic fluctuations due to 3-D sound speed perturbation in the water column. This tangent linear model will also be used for sensitivity analysis to assess the joint ocean and seabed effects.

APPROACH

The technical approaches employed in the 3D sound propagation study include theoretical analysis, numerical computation and real data analysis. A 3-D normal mode method has been used to study canonical environmental models of shelfbreak front systems [1] and nonlinear internal wave ducts [2-3]. 3-D parabolic-equation (PE) wave propagation models with improved split-step marching algorithms [4-6] are used to study sound propagation in realistic environments. When the acoustic mode coupling can be neglected, a vertical-mode horizontal-PE model is used. These PE models employ the following higher order operator splitting to increase the PE approximation accuracy.

$$\sqrt{1+\mathcal{A}+\mathcal{B}} \cong \sqrt{1+\mathcal{A}} + \left(-1+\sqrt{1+\mathcal{B}}\right) - \frac{1}{2}\left(-1+\sqrt{1+\mathcal{A}}\right)\left(-1+\sqrt{1+\mathcal{B}}\right) - \frac{1}{2}\left(-1+\sqrt{1+\mathcal{B}}\right)\left(-1+\sqrt{1+\mathcal{A}}\right), \quad (1)$$

where $\mathcal{A}$ and $\mathcal{B}$ are two different operators. In the split-step Fourier PE, they are the free-space propagator and the medium phase speed anomalies, respectively [5]. In the split-step Padé PE, they are the derivations in the horizontal and vertical directions [6].

The parabolic-equation (PE) approximation method, first introduced by Tappert [7] to underwater sound propagation modeling, has long been recognized as one of the most efficient and effective numerical methods to predict sound propagation in complex environments. The advantage of this method is due to the fact that it converts the Helmholtz wave equation of elliptic type to a one-way wave equation of parabolic type. The conversion allows efficient marching solution algorithms for solving the boundary value problem posed by the Helmholtz equation (see Figure 1). This can reduce significantly the requirement for computational resources, especially for modeling three-dimensional (3-D) sound propagation.

A higher order numerical algorithm has recently been proposed to split the square-root Helmholtz operator employed by the PE method for modeling sound propagation. This operator splitting method deals with multidimensional cross terms to yield a more accurate approximation, and, most importantly, it still permits efficient 3-D PE numerical solvers, such as the Split-Step Fourier method [5] and the Alternative Direction Implicit (ADI) Padé method [6]. The higher order operator splitting algorithm is shown in the next equation:

$$\sqrt{k_{ref}^{-2}\nabla_\perp^2 + n^2} = \sqrt{1+\varepsilon+\mu} = -1 + \sqrt{1+\varepsilon} + \sqrt{1+\mu} - \frac{1}{2}\left(-1+\sqrt{1+\varepsilon}\right)\left(-1+\sqrt{1+\mu}\right) - \frac{1}{2}\left(-1+\sqrt{1+\mu}\right)\left(-1+\sqrt{1+\varepsilon}\right), \quad (2)$$

where $k_{ref} = \omega/c_{ref}$ is the reference wavenumber, n is the index of refraction $n = c_{ref}/c = k/k_{ref}$, and $\nabla_\perp^2$ denotes the Laplacian operating on the transverse coordinates.

During the Quantifying, Predicting, and Exploiting (QPE) Uncertainty Experiment in 2009 [8-9], mobile acoustic sources were deployed to study underwater sound propagation in the area of North Mein-Hua Canyon northeast of Taiwan. With the hydrophone data received on bottom mounted vertical arrays, we can obtain transmission loss (TL) measurements [10], as well as probability of dectection, which will be briefed in the next section.

WORK COMPLETED

1. 3-D higher-order tangent linear PE model

The PE approximation is an effective numerical technique for modeling underwater sound propagation in the ocean. This technique transforms the Helmholtz wave equation into a one-way wave equation that can be solved by a variety of marching algorithms. A higher order tangent linear PE solution for the sound field variability due to small variations of the sound speed have been derived [11], and it generalizes previous formulations of Hursky et al. [12] and Smith [13] for 3-D sound

propagation and for better accuracy by employing the higher-order square root operator splitting algorithm, Eq. (1). Consider the following one-way parabolic wave equation,

$$\frac{\partial}{\partial x}u(x,y,z) = ik_{\text{ref}}\left\{-1+\sqrt{k_{\text{ref}}^{-2}\nabla_{\perp}^{2}+n^{2}(x,y,z)}\right\}u(x,y,z) \tag{3}$$

Here, the Cartesian coordinate system is selected to achieve a uniform resolution, and the parabolic wave equation can also be expressed in the same form using cylindrical coordinates. In Eq. (3), u is the demodulated sound pressure with the baseline phase removed according to the reference wavenumber k_{ref}, and n is the index of refraction with respect to the reference wavenumber. Now let $n^2 = \gamma_0 + \varepsilon\gamma_1$ and, as shown in [11], the higher-order tangent linear PE solution is

$$u(x+\Delta x) \cong e^{ik_{\text{ref}}\Delta x\mathcal{L}_0}\left[1+\frac{ik_{\text{ref}}}{2}\Delta x(1-\mathcal{L}_0)\varepsilon\gamma_1\right]u(x) \tag{4}$$

An example of 75 Hz sound propagation in an idealized slope environment is shown in Figure 2 to demostarte the accuracy of the higher order tangent linear solution.

Another example of the horizontal ducting of sound by a sound speed front over a slope is presented. The sound speed front is caused by a nonlinear internal wave of depression across the slope as shown in Figure 3(a). There are two layers in the water column, and the upper layer is 20-m thick with sound speed 1520 m/s, as opposed to 1480 m/s in the lower water layer. A 75Hz point source is placed between the apex and the internal wave (500m to the wave), and the source depth is 50 m. Figure 3(b) shows the background TL solution on the x-y plane at the source depth (50 m) in the absence of the internal wave, and one can see both the cut-off of the sound in the x direction and the interference pattern caused by the horizontal refraction of acoustic modes off the slope. Because the thermocline in the water column is depressed by the internal wave, a 3-D acoustic duct is formed. The higher-order tangent linear solution shown in Figure 3(c) indeed captures the propagation physics. To examine the accuracy of the tangent linear solution, the higher-order split-step Fourier PE solution [5] is computed directly without using the perturbation formula. As seen in Figure 3(d), the higher-order tangent linear solution agrees with the direct solution very well. Note that, even though the acoustic ducting condition changes drastically due to the presence of the internal wave, the tangent linear solution can still accurately predict the effects of sound speed variations and track down the sound field variability.

2. 3-D sound pressure sensitivity kernel

From the higher-order tangent linear PE solution (4), we can deduce the following local tangent kernel to determine the gradient of the sound pressure with respect to n^2 at a given position $\vec{x}'$.

$$\frac{\partial(p|_{\vec{x}'})}{\partial(n^2|_{\vec{x}'})} = \frac{ik_{\text{ref}}}{2}(1-\mathcal{L}_0)\,p(\vec{x}') \tag{5}$$

By incorporating the Green's function between the perturbation position $\vec{x}'$ and the receiver position $\vec{x}$, one can obtain the sensitivity kernel of the sound pressure at $\vec{x}$ due to the medium perturbation at $\vec{x}'$:

$$\frac{\partial(p|_{\vec{x}})}{\partial(n^2|_{\vec{x}'})} = G(\vec{x};\vec{x}')\frac{\partial(p|_{\vec{x}'})}{\partial(n^2|_{\vec{x}'})}. \tag{6}$$

Sensitivity analysis is implemented for an idealized Gaussian canyon model as an example.

The example showing the sound propagation effects caused by submarine canyons is done with

the 3-D Split-step Fourier PE model [5]. A strong focusing effect can be seen when sound propagates along the canyon axis (see Figure 4). In addition to the propagation study, the sensitivity kernels of sound pressure variations at three receiver locations due to medium perturbations in the canyon are shown in Figure 5. The dependency of the sensitivity kernel on receiver locations is significant. These sensitivity maps essentially tell how much the receiving sound pressure can change due to the medium perturbation at a given position.

Another example (nonlinear internal waves) showing how we can use the higher-order 3-D tangent linear PE solution to deduce a local sound pressure sensitivity kernel is shown in Figure 6. By incorporating the Green's function, we can then extend the local sensitivity kernel to the receiver position. An adjoint modeling framework has also been implemented to determine the dynamics of the sensitivity kernel associated with the physical oceanographic field. An example showing the sensitivity kernel of sound intensity with respect to sound speed perturbation, $\partial|p|^2/\partial c$, in a nonlinear internal wave field is shown in Figure 6.

3. 3-D sound propagation under non-planar surface waves

A numerical model employing the ADI Padé PE method has been developed to simulate underwater sound propagation under a non-plananr surface boundary. An illustration of the ADI method separating two-dimensional derivatives to one-dimeniosnal derivative is shown in Figure 7(a). In order to better capature the curvature of the surface boundary, a boundary-fitted grid is developed and shown in Figure 7(b), and a variable grid discrization scheme is implemented.

A semi-circular waveguide with pressure-release boundaries is employed to benchmark the numerical model. A normal mode solution consisting of Fourier-Bessel bases is first determined:

$$P(r,\phi,x) = i2\pi \sum_m \sum_n F_m(\phi_0) R_{mn}(r_0) F_m(\phi)\, R_{mn}(r) \frac{e^{i\sqrt{k^2-\kappa_{mn}^2}\,x}}{\sqrt{k^2-\kappa_{mn}^2}}, \qquad (7)$$

where the Fourier bases $F_m(\phi) = \sqrt{\frac{2}{\pi}} \sin m\phi$, the Bessel bases $R_{mn}(r) = \sqrt{2}\,\frac{J_m(\kappa_{mn} r)}{a J_{m+1}(\kappa_{mn} a)}$, and a is the radius of the waveguide. The propagation angle (inclination angle from x) can be determined by $\theta_{mn} = \cos^{-1}\left[\sqrt{k^2-\kappa_{mn}^2}/k\right]$, where $\kappa_{mn} = j_{m,n}/a$, and $j_{m,n}$ indicates zeros of the Bessel functions. We can in fact use the Fourier Bessel modes to test the higher order PE angle limit. The computation results are shown in Figure 8, and a brief discussoin is provided in the next section.

4. Joint physical oceanographic and acoustics modeling

A framework has been developed for integrating numerical models of ocean dynamics and acoustics. A data-assimilated ocean model is employed to drive the ocean dynamics in this joint model. An example of sound propagation on a shelfbreak in the Mid-Atlantic Bight is shown in Figure 9. One can see that the original down-slope propagation pattern changes to water-borne ducting due to the change of water column stratification. This examples demonstrates the use of this integrated numerical technical for studying the 3-D sound propagation effects caused jointly by physical oceanographic processes and marine geological variability.

5. 3-D sound propagation over a submarine canyon

The sound propagation effects caused by submarine canyons have also been studied in this year using the TL data collected during the QPE experiment [8-9], where mobile acoustic sources were utilized to study sound propagation over North Mein-Hua Canyon. A 3-D PE model [4] is employed to explain the underlying physics. The acoustic data show a significant decrease in sound intensity as the source crossed over the canyons (see Figure 10), and the numerical model produces comparable results due to this shadowing effect. In addition, the model suggests that 3-D sound focusing due to the canyon seafloor can occur when the underwater sound propagates along the canyon axis.

A preliminary study has been performed to examine the effects of bathymetric and bottom property uncertainties. The first environmental uncertainty to be discussed is the bathymetry, which is the most important factor causing sound field complexity over a submarine canyon. Because bathymetric errors can transfer into TL errors through incorrect bottom interaction in a sound propagation model, it is important to have an accurate bathymetric map to ensure model accuracy. To examine the pre-QPE bathymetric database, the water depth data obtained from shipboard echo sounders during the 2009 QPE cruises were compared, and a specific comparison (Figures 8(d) and 8(e)) is made to show the difference in the modeled TL that result from using the two different bathymetric data sets. The propagation path runs across the canyon, and the two bathymetric datasets indeed produce different TL predictions. The most notable discrepancy is the interference pattern near the start of the track, but both models produce comparable shadow zones ranging from 4 to 7 km and extending to 200 m deep. This explains why the data and model comparison using the pre-QPE bathymetric database shows reasonable agreement. Also note the bottom reflection in the steep canyon (Figure 10(e)). Although the up-slope propagation terminates the shadow zone, the TL is large because the steep slope causes greater bottom loss.

The next environmental uncertainty to be considered is the bottom geoacoustic properties. Based on the understanding of strong currents in the canyon area, fine suspended sediments are not supposed to settle easily. So, a sandy bottom model is assumed for the numerical simulations with sound speed *cp* 1700 m/s, density 1.5 g/cm3 and attenuation coefficient 0.5 dB/λ. To present changes of the modeled TL due to different bottom properties, the same numerical computation is repeated with two other bottom sound speeds, 1600 m/s and 1800 m/s. The modeled TL distributions are shown in Figures 3(f) and 3(g) with comparisons to the measured mean TL data. The bottom model with *cp* = 1800 m/s does improve the TL comparison. This suggests that the real bottom is probably harder than what we expect, or that the bottom is more variable (i.e., consists of a number of different regimes) than was assumed. To make a stronger statement, we need to consider the bathymetric uncertainty that can also affect the predictability of bottom reflections. Such a joint uncertainty study will be performed later in the project.

5. Probability of dection of sound over a submarine canyon

The QPE canyon transmission data have also been used to obtain the probability of detection of sound over North Mien Hua Canyon (see Figure 11). The data processing method is briefed here. In each 1-min transmission, there were six 2-s HFM sweeps and 48-s long CW tones. A portion of the acoustic data during the CW transmission (30 s) is processed with the short-time Fourier transform (STFT) to detect the 880 Hz CW signal. In each STFT step, a 2-s long signal is extracted and tapered with a Hamming window. It is then zero-padded to be ~13.4-s long to produce a high-resolution

spectrum around the nominal frequency (880 Hz). The location of the greatest spectrum peak is recorded for computing the signal detection rate. To continue the process until the end of the 30-s data, the STFT window is moved in a 1-s interval, which results in totally 30 spectrum measurements. The ratio of the greatest peak of each spectrum locating within +/-0.5 Hz around the theoretical Doppler-shifted frequency is calculated, and it is the probability of detection of the 880Hz signal. The cross dots in Figure 11(c) are in fact the measured probability for every transmission within the processed window bounded by the lines shown in Figure 10(a). Note that the decreasing of the detection probability seen in Figure 10(c) is in fact caused by the shadowing effect of the sound propagating across the canyon explained in the preceding section.

6. Horizontal ducting of sound in a meandering internal wave duct

A numerical computation of horizontal ducting of sound in a meandering nonlinear internal wave field has been made. The wavefronts follow a sinusoidal function with a 200-m amplitude and a 20-km wave length. The internal wave curvature is 50.66 km at the most curved part, and it changes longitudinally along the duct. As sketched in Figure 12(a), the horizontal modes tend to be of whispering gallery type in the most curved part. On the other hand, the horizontal modes tend to be fully bouncing in the less curved portion because the concavity of the wavefront is not great enough to support whispering gallery ducting. Figures 12(b)–12(e) depict the horizontal ducting of vertical modes 1 and 2 for different source locations obtained from 3-D PE calculations. In this example where the source is placed in the curved part, when the source is close to the outer wave, more sound is trapped in the duct. This is because the whispering gallery modes in the curved part are excited. In this meandering wave case, we also notice that the horizontal modes have a longitudinal variation, because the internal wave curvature changes along the waveguide. In a more realistic situation, where the wave shape varies along the wavefront, the horizontal mode variation will be even more significant. The consequence is that the ducted sound will encounter horizontal mode coupling.

7. Engineering test in the New England Mud Patch area

The PI also joined an engineering test on the New England Mud Patch, south of Martha's Vineyard, MA for examing propagation conditions of broadband acoustic pulses generated by a combustive sound source deployed by ARL:UT. One of the hydrophone arrays deployed in this test was provided by the PI and the acoustics group at WHOI. Preliminary acoustic data and model analyses are shown in Figure 13. Sound propagation models in two different sediment types of environments are shown in Figures 13(a) and 13(b). The sound source in this modeling study is placed close to the seafloor. In Figure 13(a), the sediment layer is modeled as fine-granted sediment (mud) with compressional wave speed less than the sound speed in the bottom of water. In Figure 13(b), the sediment layer is modeled as sand with higher compressional wave speed. The model clearly shows that the acoustic energy can be trapped in the lower speed mud layer. A preliminary broadband pulse data and model comparison is shown in Figures 13(c) and 13(d). In Figure 13(c), the spectrograms of received pulses on the hydrophone array are shown, along with time series plots in the bottom panel. In Figure 13(d), results from a broadband sound propagation model are shown. The sediment layer in the model is made to be mud. Despite the very low frequency ground waves, this preliminary model adequately reproduces the pulse dispersion over a broad frequency range.

RESULTS

The major results of this project are summaried here, along with a publication list provided later. First, A higher-order tangent linear PE solution of 3D sound propagation has been derived, and it unifies other tangent linear PE solutions by employing a higher-order splitting algorithm for the square-root Helmholtz operator. Numerical examples of 3D sound propagation are presented to show the performance of the solution. The first example considers an idealized slope/wedge problem (Figure 2), and the higher-order tangent linear solution agrees very well with the reference solution obtained from the method of images. The second example (Figure 3) is the horizontal ducting of sound by a sound speed front over a slope. It shows that the tangent linear solution can accurately predict the sound field variability even when the ducting condition changes drastically.

This higher-order tangent linear solution also yields a sensitivity kernel of sound pressure variations due to changes in medium sound speed. Numerical examples of 3D sound propagation in an idealized Gaussian canyon are presented to show the performance of the solution in Figures 4 and 5. The examples clearly show the focusing effect for sound propagation along the canyon axis and the spatial distribution of the sound pressure sensitivity. An adjoint modeling has also implemented to study the dynamics of the sensitivity kernel associated with the physical oceanographic field. An numerical example of 3-D sound pressure sensitivity analysis in a nonlinear internal wave field is presented (Figure 6).

A 3D sound propagation model with non-planar surface has been developed. The applications of this model will include studies of 3D propagating sound scattered from rough sea surface. A benchmark problem of semi-circular waveguides is employed to validate the model, and the benchmarking result is excellent. Numbers from error analyses are provided in the caption of Figure 8.

Theoretical and numerical investigations of 3D sound propagation have been carried out to study effects due to meandering nonlinear internal waves. The study shows that the horizontal ducting of sound by curved internal waves has generally two types: whispering gallery modes and fully bouncing modes, and in order for the sound to be ducted by the meandering waves, the whispering gallery modes in the curved part need to be excited.

The QPE transmission data have been analyzed for sound propagation over the North Mien-Hua Canyon northeast of Taiwan. A pre-cruise numerical study showed a strong 3-D focusing effect caused by the concave canyon seafloor. Mobile acoustic sources were deployed to validate the model. However, the sources were pushed off of their planned tracks by the current, so we were not able to confirm the predicted focusing effect. Nonetheless, the field data still showed a shadowing effect, which is also an important factor in considering underwater sound propagation over a submarine canyon. A 3-D PE model was utilized to provide physical insights into the TL data. Acoustic shadow zones are identified in the numerical model, and the resultant shadowing effect agrees with the measured data quite well. Model uncertainties due to incomplete measurements of the sound speed field, the seafloor topography and the sub-bottom structure are also noted, and it is left for future work to thoroughly evaluate the effect of each environmental uncertainty on the TL predictability. Bathymetric uncertainty could be the most important factor when considering sound propagation in a submarine canyon, and it will affect the TL predictions in conjunction with other environmental uncertainties.

A numerical model has been constructed to include the sub-bottom layering structure. The purpose of this integrated model is to investigate the 3D sound propagation effects caused jointly by

marine geological features and oceanographic dynamics in shallow water. This integrated model will also be used to study the sound pressure sensitivity due to time-varying water column dynamics. Aligning with this research topic, the PI joined an engineering test on the New England Mud Patch for a preliminary sound propagation study. The initial data analysis and modeling effort is presented in Figure 13. In addition to that, ambient noise analysis has been initiated. Figure 14 shows the noise spectrum level during container ships passing by the acoustic engineering test site. The nominal closest-point-of-approach (CPA) distance to the hydrophone array was about 5 to 7 km. The hydrophone deployment was 5.5 days, and the noise spectrum within a 2 hour time window around every CPA are analyzed. Total 35 containers were detected acoustically, and the total analyzed time for the ambient noise was 65 hours long. In Figure 14, the black lines denote the mean and one standard deviation curves. The color curves are the average levels of heavy, moderate and light shipping noise in deep ocean [14]. The analysis suggests that when the big container ships pass by, the ambient noise can reach up to 110 dB re 1μ Pa at frequencies around 100 Hz, which is 30 dB more than the average level in deep ocean reported by Urick [14] for heavy shipping.

IMPACT/APPLICATIONS

The potential relevance of this work to the Navy is on increasing the capability of sonar systems in shallow water areas. The contributions of the effort on studying 3-D sound propagation effects will also be on assessing the environment-induced acoustic impacts.

RELATED PROJECTS

Experimental data used in this project were collected from the ONR SW06 and QPE projects and one of the the reconnaissance cruises on the New England Mud Patch. In addition, strong collaborations have been initiated and continued between the PI's of an ONR MURI project on integrated ocean dynamics and acoustics.

REFERENCES

[1] Y.-T. Lin and J.F. Lynch, "Analytical study of the horizontal ducting of sound by an oceanic front over a slope, " *J. Acoust. Soc. Am.*, vol. 131, pp. EL1-EL7 (2012).

[2] Y.-T Lin, T.F. Duda and J.F. Lynch, "Acoustic mode radiation from the termination of a truncated nonlinear internal gravity wave duct in a shallow ocean area", *J. Acoust. Soc. Am.*, vol. 126, pp. 1752-1765 (2009).

[3] Y.-T. Lin, K.G. McMahon, J.F. Lynch, and W.L. Siegmann, "Horizontal ducting of sound by curved nonlinear internal gravity waves in the continental shelf areas," *J. Acoust. Soc. Am.*, vol. 133, pp. 37-49 (2013).

[4] Y.-T. Lin, T.F. Duda, and A.E. Newhall, "Three-dimensional sound propagation models using the parabolic-equation approximation and the split-step Fourier method," *J. Comp. Acoust.*, vol. 21, 1250018 (2013).

[5] Y.-T. Lin and T.F. Duda, "A higher-order split-step Fourier parabolic-equation sound propagation solution scheme," *J. Acoust. Soc. Am*, vol. 132, pp. EL61-EL67 (2012).

[6] Y.-T. Lin, J.M. Collis and T.F. Duda, "A three-dimensional parabolic equation model of sound propagation using higher-order operator splitting and Padé approximants," *J. Acoust. Soc. Am.*, vol. 132, pp. EL364-370 (2012).

[7] F. D. Tappert, Parabolic equation method in underwater acoustics, *J. Acoust. Soc. Am.*, vol. 55, p. S34 (1974).

[8] Gawarkiewicz, G. G., S. Jan, P. F. J. Lermusiaux, J. L. McClean, L. Centurioni, K. Taylor, B. 14 Cornuelle, T. F. Duda, J. Wang, Y. J. Yang, T. Sanford, R.-C. Lien, C. Lee, M.-A. Lee, W. 15 Leslie, P. J. Haley Jr., P. P. Niiler, G. Gopalakrishnan, P. Velez-Belchi, D.-K. Lee, and Y. Y. 16 Kim (2011). "Circulation and intrusions northeast of Taiwan: Chasing and predicting 17 uncertainty in the cold dome," *Oceanography*, vol. 24, pp. 110-121.

[9] A.E. Newhall, J.F. Lynch, G.G. Gawarkiewicz, T.F. Duda, N.M. McPhee, F.B. Bahr, C.D. Marquette, Y.-T. Lin, S. Jan, J. Wang, C.-F. Chen, L. Y.-S. Chiu, Y.-J. Yang, R.-C. Wei, C. Emerson, D. Morton, T. Abbot, P. Abbot, B. Calder, L.A. Mayer, and P.F.J. Lermusiaux, Acoustics and oceanographic observations collected during the QPE Experiment by Research Vessels OR1, OR2 and OR3 in the East China Sea in the Summer of 2009, Woods Hole Oceanographic Institution Tech. Report WHOI-2010-06, Woods Hole Oceanographic Institution, Woods Hole, MA, USA.

[10] Y.-T. Lin, T.F. Duda, C. Emerson, G.G. Gawarkiewicz, A.E. Newhall, B. Calder, J.F. Lynch, P. Abbot, Y.-J. Yang and S. Jan, "Experimental and numerical studies of sound propagation over a submarine canyon northeast of Taiwan," *IEEE J. Ocean. Eng.*, vol. 40, pp. 237-249 (2015).

[11] Y.-T. Lin, "A higher-order tangent linear parabolic-equation solution of three-dimensional sound propagation, " *J. Acoust. Soc. Am.*, vol. 134, pp. EL251-EL257 (2013).

[12] P. Hursk, M. B. Porter, B. D. Cornuelle, W. S. Hodgkiss, and W. A. Kuperman, "Adjoint modeling for acoustic inversion," *J. Acoust. Soc. Am.*, vol. 115, 607–619 (2004)

[13] K. B. Smith, "Adjoint modeling with a split-step Fourier parabolic equation model (L)," *J. Acoust. Soc. Am.*, vol. 120, 1190–1191 (2006).

[14] Urick, Robert, Principles of Underwater Sound, International Edition (McGraw-Hill, Inc.), Chap. 7, 1993.

PUBLICATIONS

1. Peer refereed papers

2015 A.A. Shmelev, J.F. Lynch and **Y.-T. Lin**, "Low frequency acoustic propagation through crossing internal waves in shallow water," *J. Acoust. Soc. Am.*, [submitted, referred]

2015 B.J. DeCourcy, **Y.-T. Lin**, and W.L. Siegmann, "Approximate formulas and physical interpretations for horizontal acoustic modes in a shelf-slope front model," *J. Acoust. Soc. Am. Express Letter*, [accepted, referred]

2015 **Y.-T. Lin**, T.F. Duda, C. Emerson, G.G. Gawarkiewicz, A.E. Newhall, B. Calder, J.F. Lynch, P. Abbot, Y.-J. Yang and S. Jan, "Experimental and numerical studies of sound propagation over a submarine canyon northeast of Taiwan," *IEEE J. Ocean. Eng.*, vol. 40, pp. 237-249. [published, refereed]

2015 C. Emerson, J.F. Lynch, P. Abbot, **Y.-T. Lin**, T.F. Duda, G.G. Gawarkiewicz and C.-F. Chen, "Acoustic Propagation Uncertainty and Probabilistic Prediction of Sonar System Performance in the Southern East China Sea Continental Shelf and Shelfbreak Environments," *IEEE J. Ocean. Eng.*, vol. 40, pp. 1003-1017. [published, refereed]

2015 L.Y.S. Chiu, A. Chang, **Y.-T. Lin**, and C.-S. Liu, "Estimating Geo-acoustic Properties of the Surficial Sediments in the Region of North Mein-Hua Canyon with a Chirp Sonar Profiler," *IEEE J. Ocean. Eng.*, vol. 40, pp. 222-236. [published, refereed]

2014 A.A. Shmelev, J.F. Lynch, **Y.-T. Lin** and H. Schmidt, "3D coupled mode analysis of internal-wave acoustic ducts," *J. Acoust. Soc. Am.*, vol. 135, pp. 2497-2512. [published, refereed]

2013 **Y.-T. Lin**, "A higher-order tangent linear parabolic-equation solution of three-dimensional sound propagation," *J. Acoust. Soc. Am.*, vol. 134, pp. EL251-EL257. [published, refereed]

2103 **Y.-T. Lin**, T.F. Duda, and A.E. Newhall, "Three-dimensional sound propagation models using the parabolic-equation approximation and the split-step Fourier method," *J. Comp. Acoust.*, vol. 21, 1250018.

2013 **Y.-T. Lin**, K.G. McMahon, J.F. Lynch, and W.L. Siegmann, "Horizontal ducting of sound by curved nonlinear internal gravity waves in the continental shelf areas," *J. Acoust. Soc. Am.*, vol. 133, pp. 37-49. [published, refereed]

2. First-author meeting proceeding and short abstract

2015 **Y.-T. Lin**, "Higher order square-root Helmholtz operator splitting," in *Proceedings of the 12th International Conference on Theoretical and Computational Acoustics (ICTCA 2015)*, Oct 11-16, 2015, Zhejiang, China. [published, not refereed] ***(Invited Paper)***

2015 **Y.-T. Lin**, "3-D Shallow Water Acoustics," in Seabed and Sediment Acoustics: Measurements and Modelling 2015, Institute of Acoustics, University of Bath, UK, Sept. 7-9 2015. [published, not refereed]

2015 **Y.-T. Lin**, "Three-dimensional parabolic-equation solutions with boundary-fitted grids," *J. Acoust. Soc. Am.*, vol. 137, p. 2421. [published, not refereed]

2015 **Y.-T. Lin** and M. J. Isakson, "Three-dimensional underwater sound propagation: Proposed benchmark problems," *J. Acoust. Soc. Am.*, vol. 137, p. 2420. [published, not refereed]

2014 **Y.-T. Lin**, " Numerical applications of a higher order square-root Helmholtz operator splitting method on modeling three-dimensional sound propagation," in Proceedings of the 2nd International Conference and Exhibition on Underwater Acoustics, June 22-27, 2014, Rhodes, Greece. [published, not refereed]

2014 **Y.-T. Lin**, A. E. Newhall, and J. F. Lynch, "Applications of an adaptive back-propagation method for passive acoustic localizations of marine mammal sounds," *J. Acoust. Soc. Am.*, vol. 136, p. 2093. [published, not refereed]

2014 **Y.-T. Lin**, "Sensitivity analysis of three-dimensional sound pressure fields in complex underwater environments," *J. Acoust. Soc. Am.*, vol. 136, p. 2121. [published, not refereed] ***(Invited Paper)***

2014 **Y.-T. Lin**, D. Barclay, T. F. Duda, and W. G. Zhang, "Three dimensional underwater acoustic modeling on continental slopes and submarine canyons," *J. Acoust. Soc. Am.*, vol. 136, p. 2317. [published, not refereed] ***(Invited Paper)***

2014 **Y.-T. Lin**, "Numerical modeling of three-dimensional underwater sound propagation under rough sea surfaces," *J. Acoust. Soc. Am.*, vol. 135, p. 2429. [published, not refereed]

2013 **Y.-T. Lin**, W. G. Zhang, and T. F. Duda, "Sensitivity of the underwater sound field in submarine canyons to water column variability," *J. Acoust. Soc. Am.*, vol. 134, p. 4114. [published, not refereed]

2013 M.E.G.D. Colin, T.F. Duda, L.A. te Raa, T. van Zon, P.J. Haley Jr., P.F.J. Lermusiaux, W.G. Leslie, C. Mirabito, F.P.A. Lam, A.E. Newhall, **Y.-T. Lin**, and J.F. Lynch, "Time-evolving acoustic propagation modeling in a complex ocean environment," in Proceedings of Oceans '13 (Bergen) Conference, IEEE/MTS. [published, not refereed]

2013 T.F. Duda, **Y.-T. Lin** and B. D. Cornuelle, Scales of time and space variability of sound fields reflected obliquely from underwater slopes, Proc. Meet. Acoust., 19, 070025. [published, not refereed]

2013 J.F. Lynch, **Y.-T. Lin**, T. F. Duda and A. E. Newhall, "Characteristics of acoustic propagation and scattering in marine canyons", in Proceedings of the 1st International Underwater Acoustics Conference, Corfu, Greece. [published, not refereed]

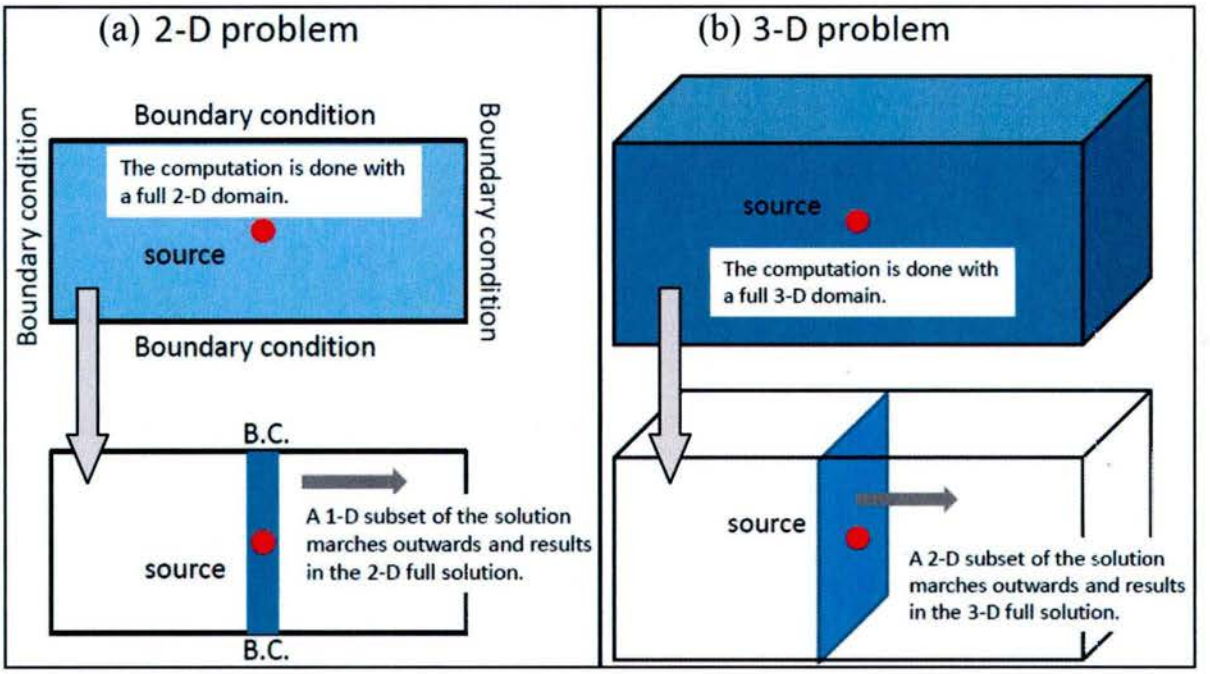

Figure 1. Dimension reduction of the Helmholtz equation by the parabolic-equation approximation. [The parabolic-equation (PE) approximation method has long been recognized as one of the most efficient and effective numerical methods to predict sound propagation in complex environments. This method approximates the Helmholtz wave equation of elliptic type to a one-way wave equation of parabolic type. The conversion allows efficient marching solution algorithms for solving the boundary value problem posed by the Helmholtz equation.]

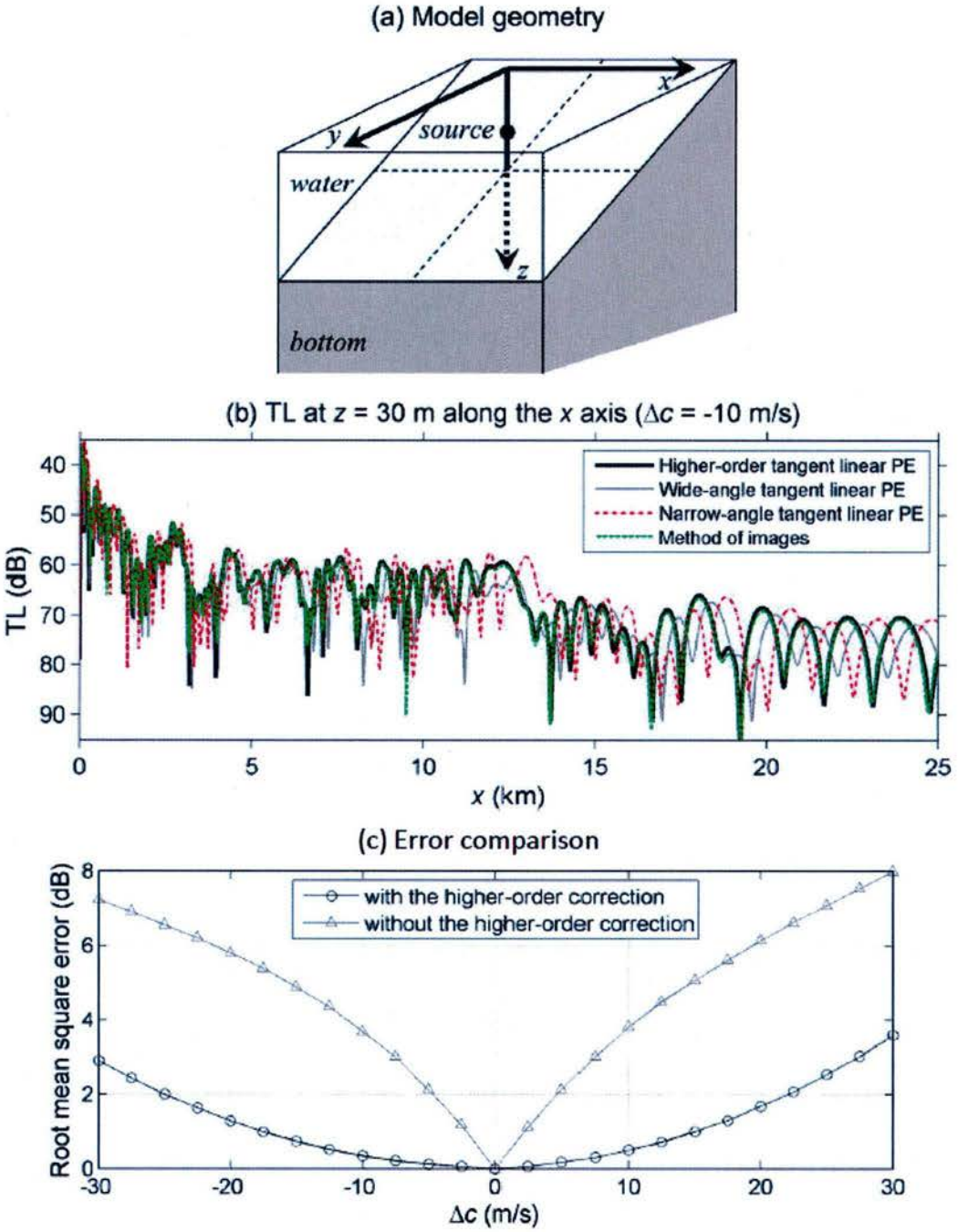

Figure 2. An example of 75 Hz sound propagation in an idealized slope environment the higher order tangent linear PE method.
[(a) Geometry of the slope model. (b) Comparison of Transmission loss (TL) solutions at z = 30m along the x axis. Among three different tangent linear PE solutions, the higher-order one has the best agreement with the reference solution obtained from the method of images. (c) Error comparison of the higher-order tangent linear PE solution with and without the higher-order correction.]

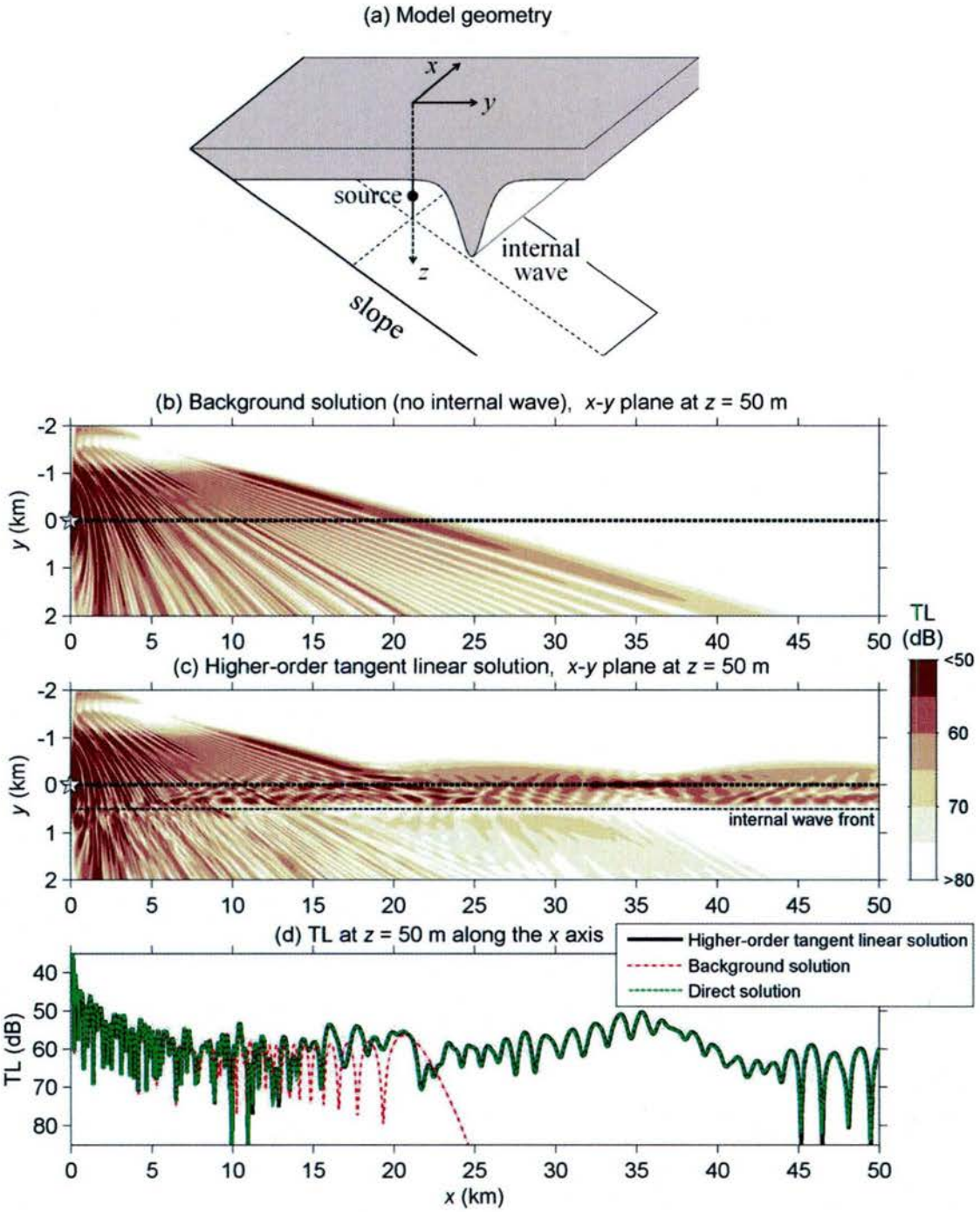

Figure 3. An example of 75 Hz sound propagation in the presence of a nonlinear internal wave over a slope.

[(a) Geometry of the slope plus internal wave model. (b) The background solution of the TL on the x-y plane at z = 50m in the absence of the internal wave. (c) The higher-order tangent linear PE solution of the TL on the x-y plane at z = 50m in the presence of the internal wave. (d) Comparison of different TL solutions.]

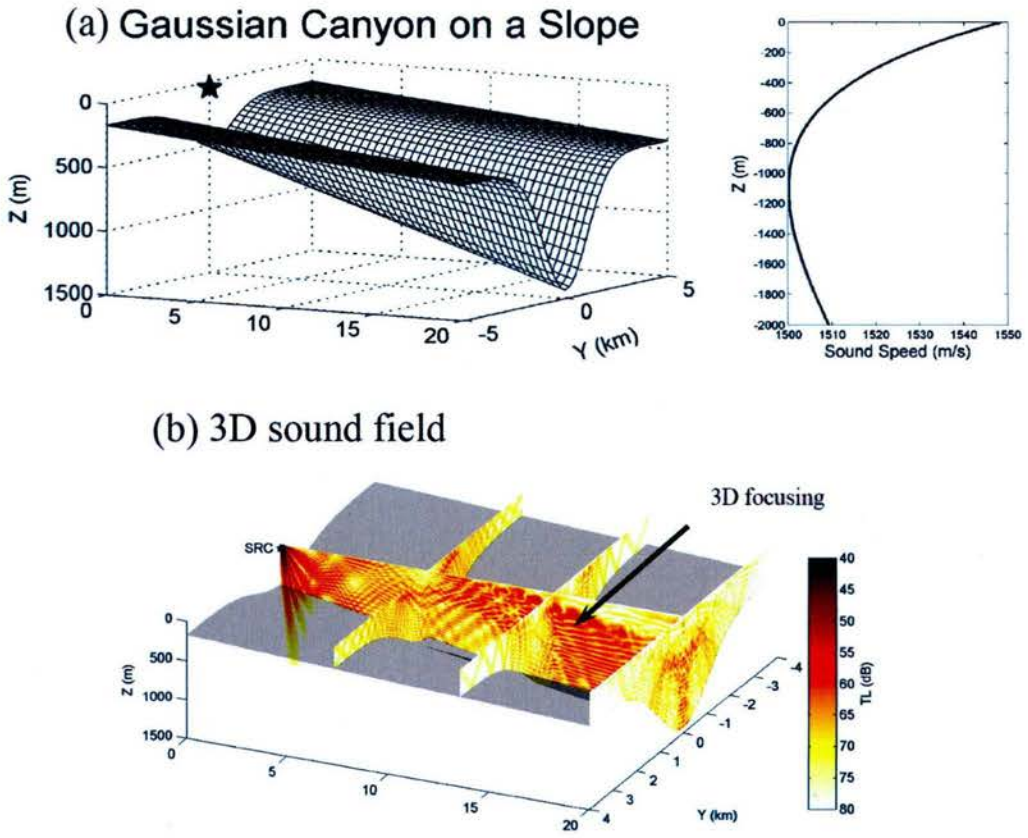

Figure 4. Idealized Gaussian canyon model.
[(a) Geometry of the canyon model. (b) The 3D sound field excited by a point source placed at the canyon axis, and strong 3D focusing effect is observed.]

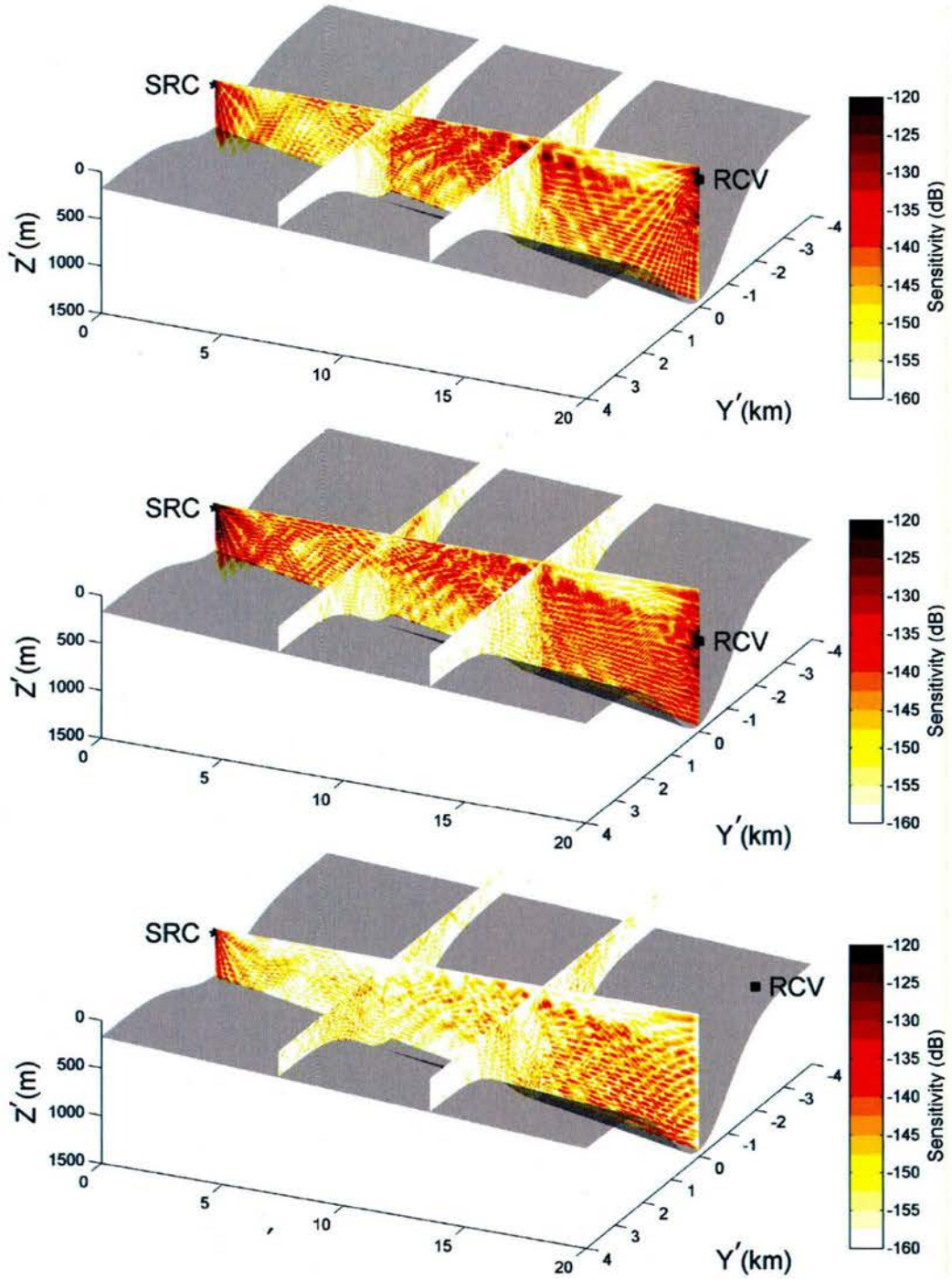

Figure 5. The sensitivity kernels of sound pressure variations at three receiver locations due to medium perturbations in the idealized Gaussian canyon model.
[One can see intensified sensitivity caused by the 3D focusing of sound. The dependency of the sound pressure sensitivity on receiver locations is significant. These sensitivity kernel maps essentially present how much the receiving sound pressure changes due to the medium perturbation at a given position.]

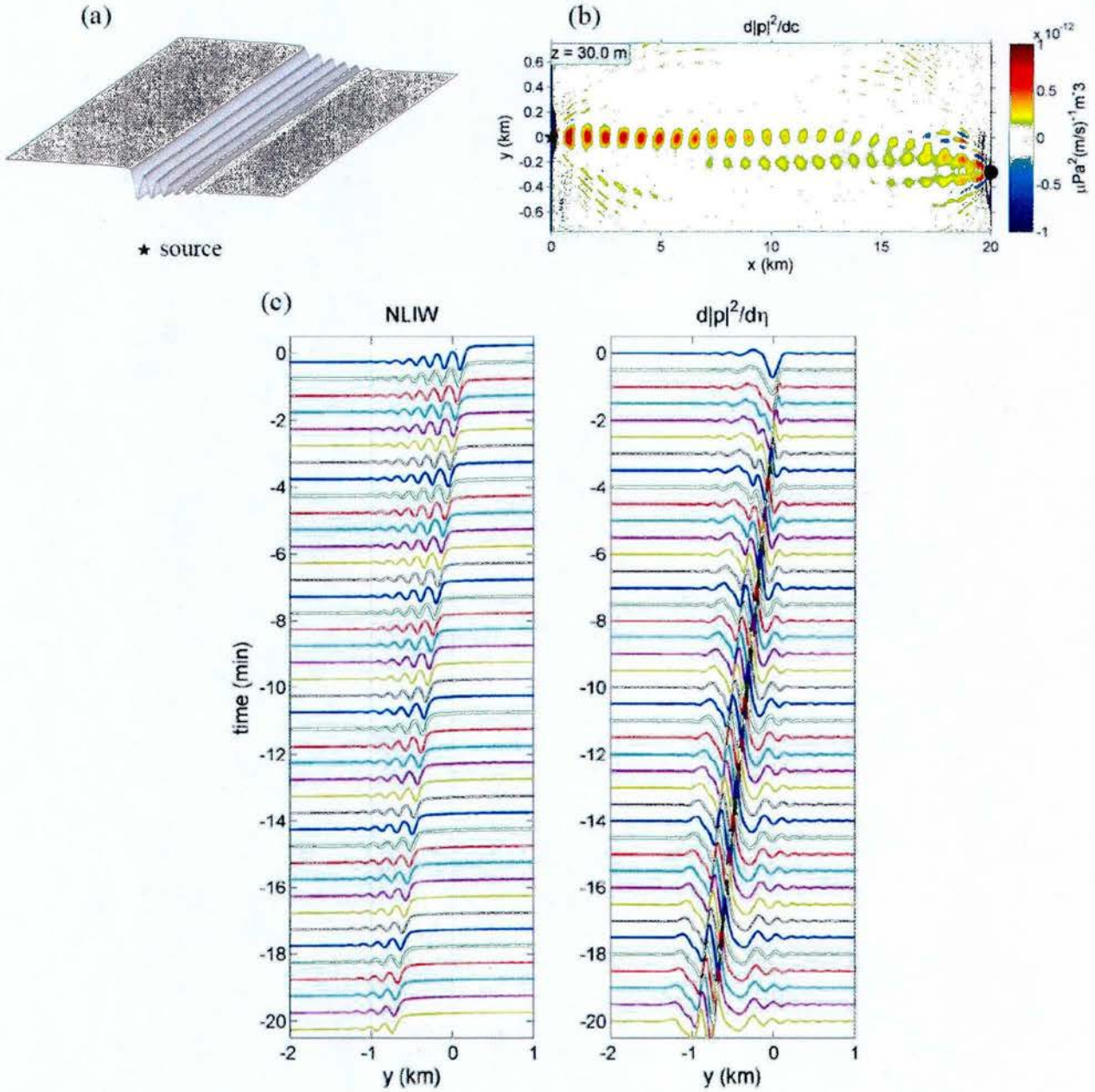

Figure 6: Sensitivity analysis of an internal wave acoustic duct. [(a) internal wave displacement (the source is underneath the first wave crest), (b) the sensitivity kernel of sound pressure square with respect to sound speed perturbation between the source and a receiver underneath the second wave crest, and (c) the sound pressure sensitivity and its dynamics following the internal wave motion. The sensitivity kernel has been converted to be per wave height through a chain rule.]

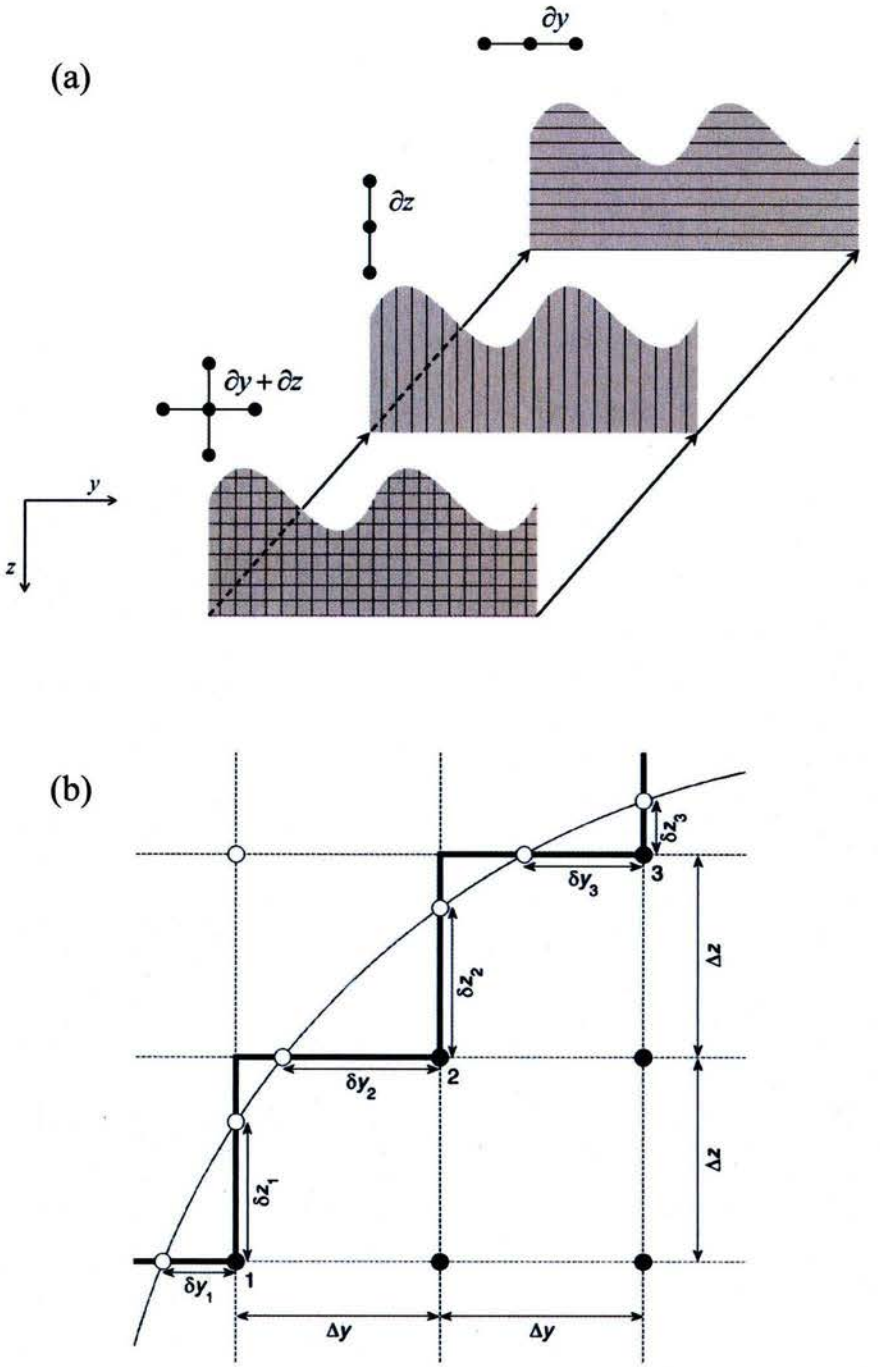

Figure 7. (a) The alternating direction implicit (ADI) method with a nonpanar surface, and (b) the boundary fitted grid for handling surface wave boundary conditions.

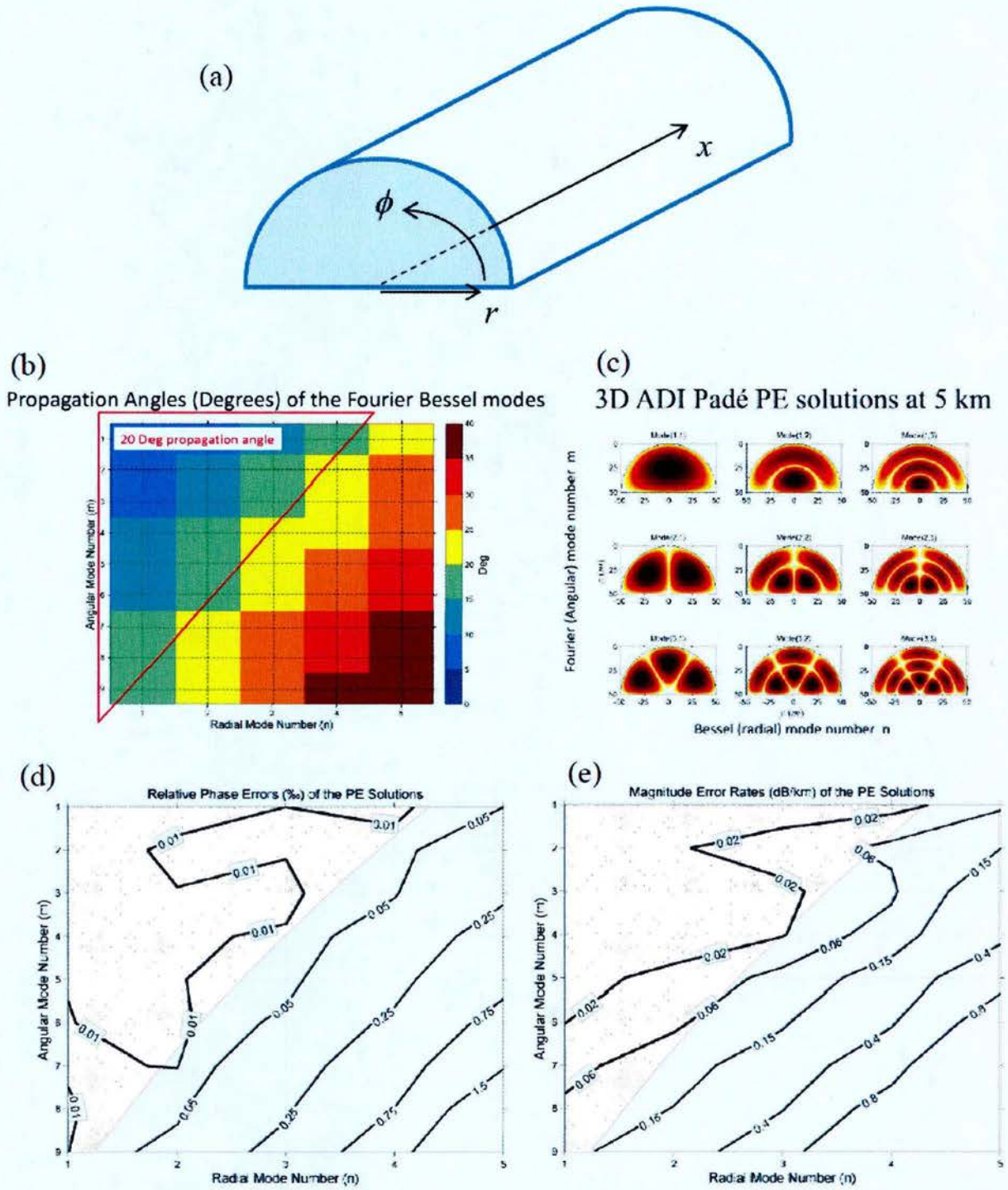

Figure 8. The semi-circular waveguide benchmark problem for the ADI Padé PE model with non-planar surface boundaries.
[(a) the gemetry of the benchmark problem, (b) the propagation angles of the Fourier-Bessel modes, (c) 3D ADI Padé PE solutions at 5 km, (d) relative phase errors (as small as 0.01 ‰), and (e) magnitude error rates (as small as 0.02 dB/km)]

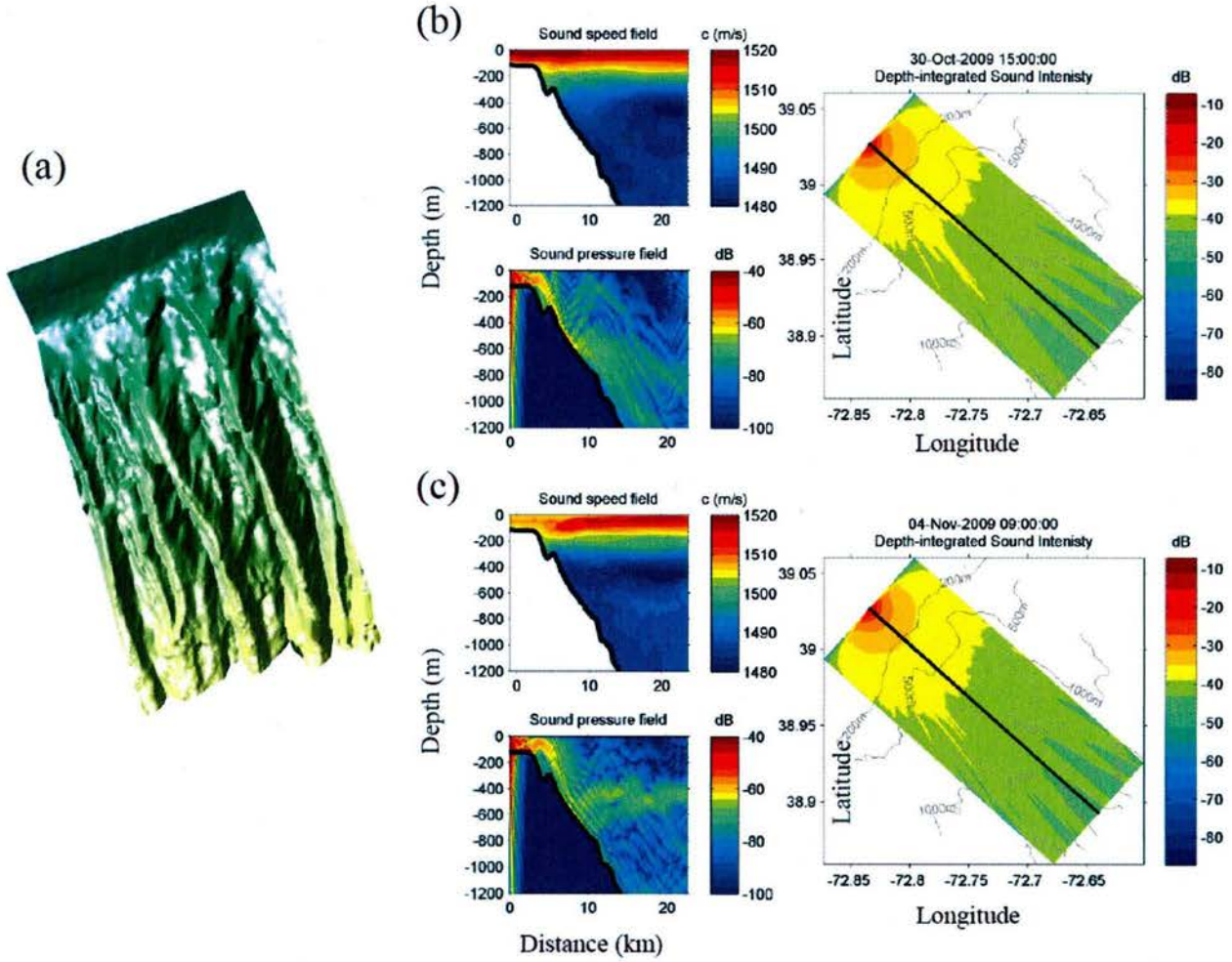

Figure 9: Integrated numerical simulations of ocean dynamics and acoustics on the slope of the New Jersey Shelf.

[(a)The bathymetry, (b) the original down-slope propagation pattern, and (c) change of propagation pattern to water-borne ducting due to water column variability. The beam pattern on the depth integrated sound intensity plots on the right shows the 3-D focusing of sound by the small canyons on the slope.]

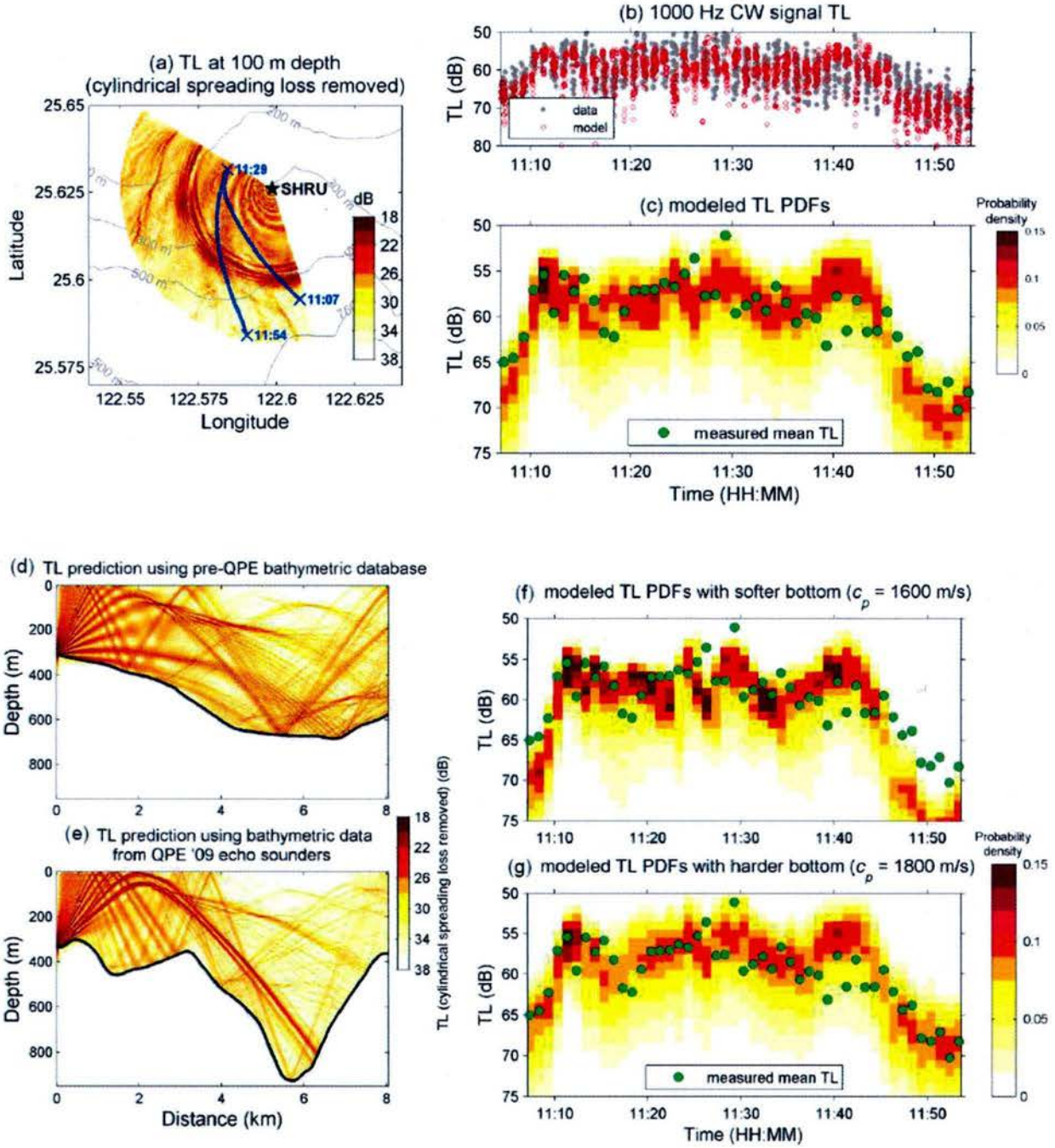

Figure 10. 3-D PE model TL and data comparison for the mobile source transmission in the QPE experiment over North Mein-Hua Canyon.

[The source track is denoted by the blue line in panel (a). The PE model TL and data are compared in a scatter plot (b) and a distribution (c). Panels (d) and (e) show the comparison of TL predictions resulted from two different bathymetric data. Panels (f) and (g) show the comparison of TL predictions resulted from two different bottom models. The bottom sound speed in the model shown in panel (c) is 1700 m/s.]

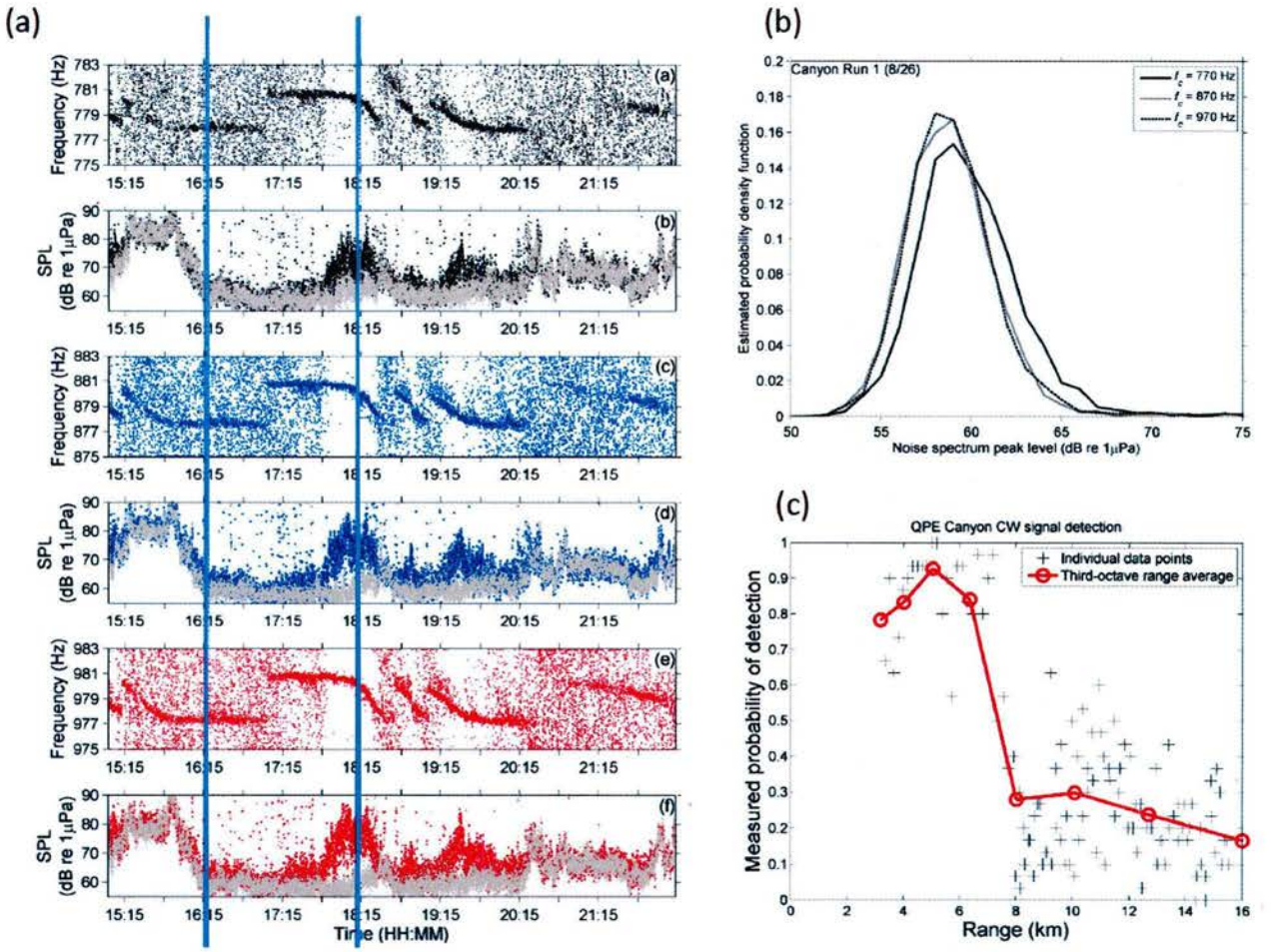

Figure 11. Probability of detection of sound over a submarine canyon. [(a) QPE canyon transmission data at three frequencies. The detected frequencies and sound pressure levels are shown. (b) The noise level distribution. (c) The cross dots are the measured probability for every transmission within the processed window between the lines in panel (a).]

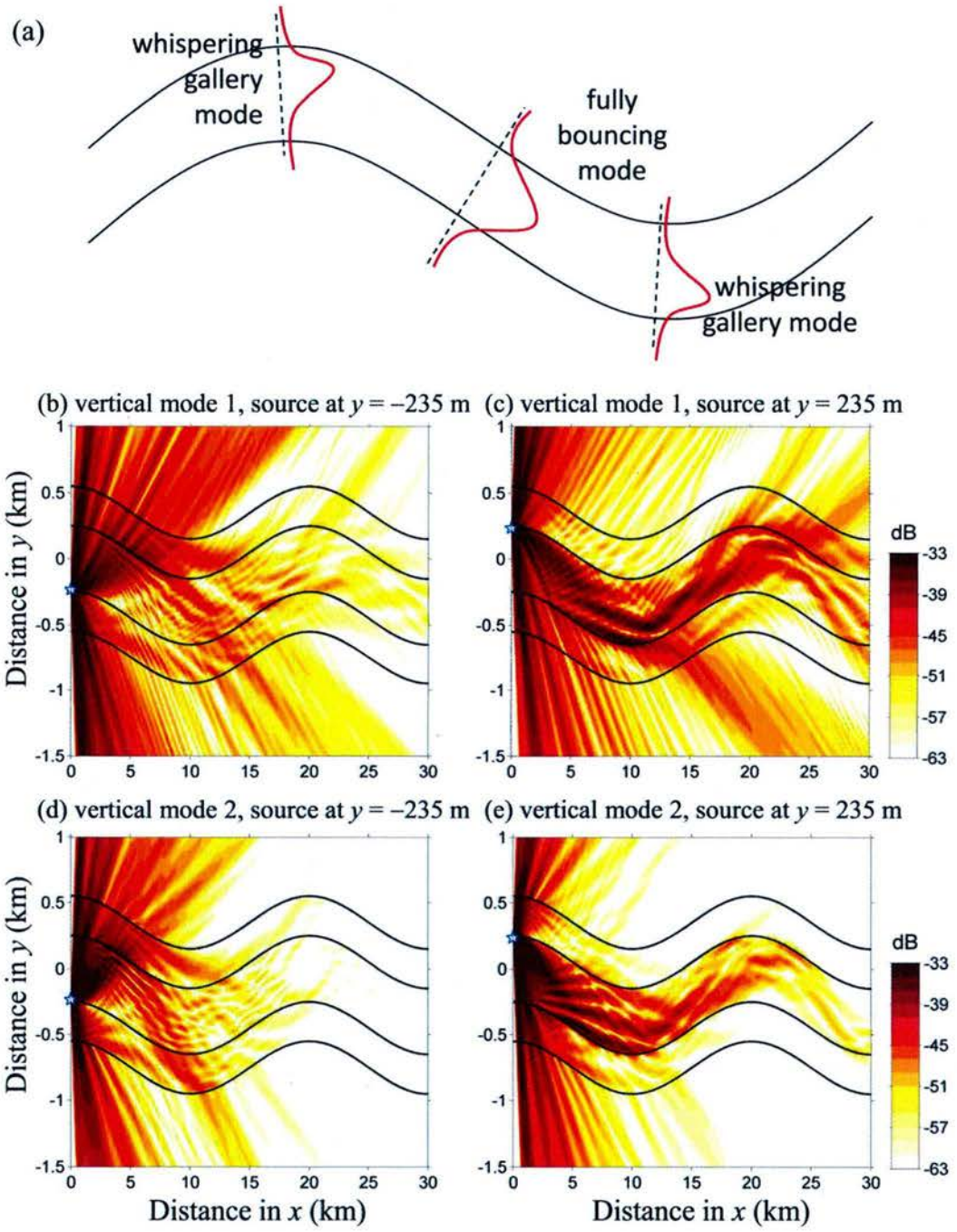

Figure 12. Horizontal ducting of sound in a meandering internal wave duct. [(a) A sketch showing different types of ducted modes in the duct. Full 3-D acoustic fields for a source in a curved portion and located (b) near the inner wave, and (c) near the outer wave. (d) Same as (b) except vertical mode 2 is plotted. (e) Same as (c) except vertical mode 2 is plotted.]

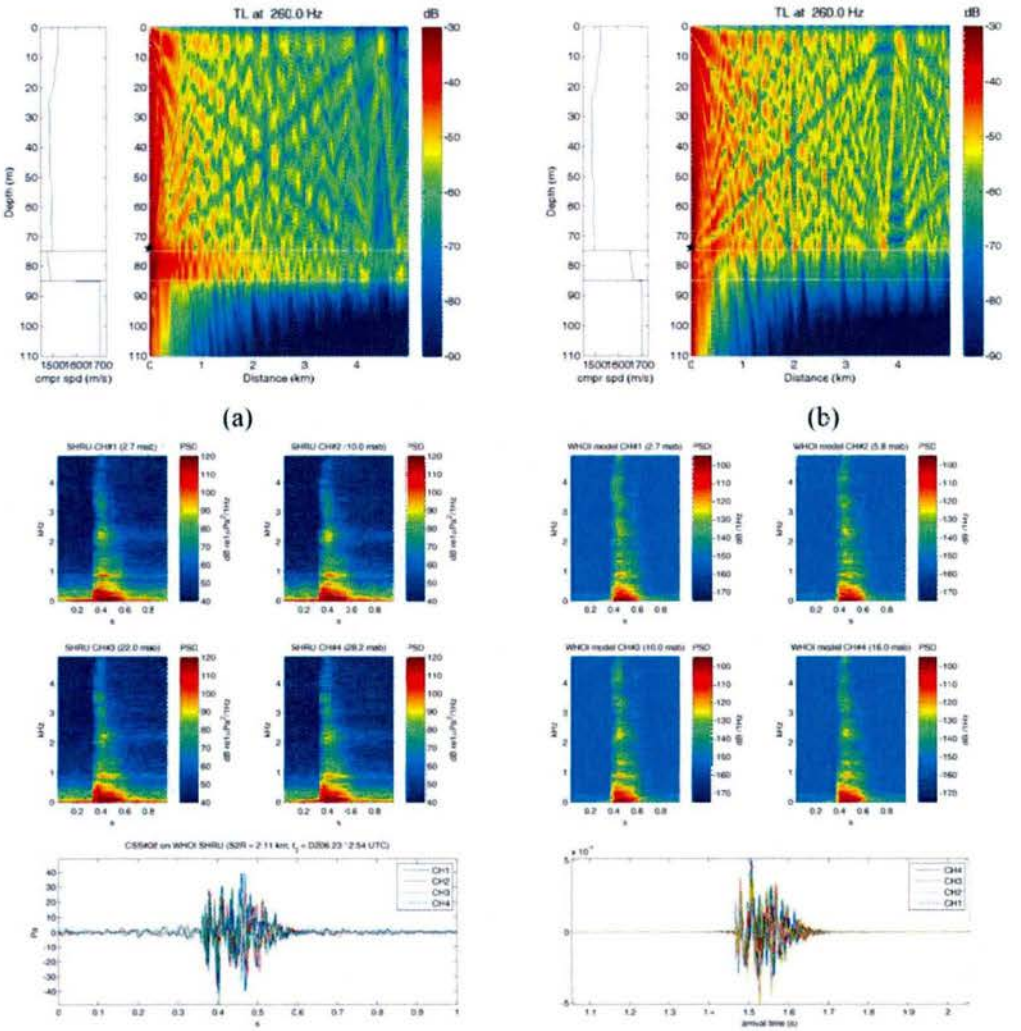

Figure 13: Preliminary acoustic data and model analyses in the engineering test conducted on the New England Mud Patch.

[(a) and (b) Sound propagation models in two different sediment types of environments. The sound source in this model study is placed close to the seafloor. In the panel (a), the sediment layer is modeled as fine-granted sediment (mud) with compressional wave speed less than the sound speed in the bottom of water column. In the panel (b), the sediment layer is modeled as sand with higher compressional wave speed. One can see that the acoustic energy can be trapped in the lower speed mud layer. (c) and (b) Preliminary broadband pulse data and model comparison. In the panel (c), the spectrograms of received pulses on four hydrophones close to the bottom are shown, along with time series plots in the bottom panel. The broadband source was made available by D. Knobles of ARL:UT, and the hydrophone array data was provided by the ocean acoustics group at WHOI. In the panel (d), results from a broadband sound propagation model are shown. The sediment layer in the model is made to be mud. Despite the very low frequency ground waves, this preliminary model adequately reproduces the pulse dispersion over a broad frequency range.]

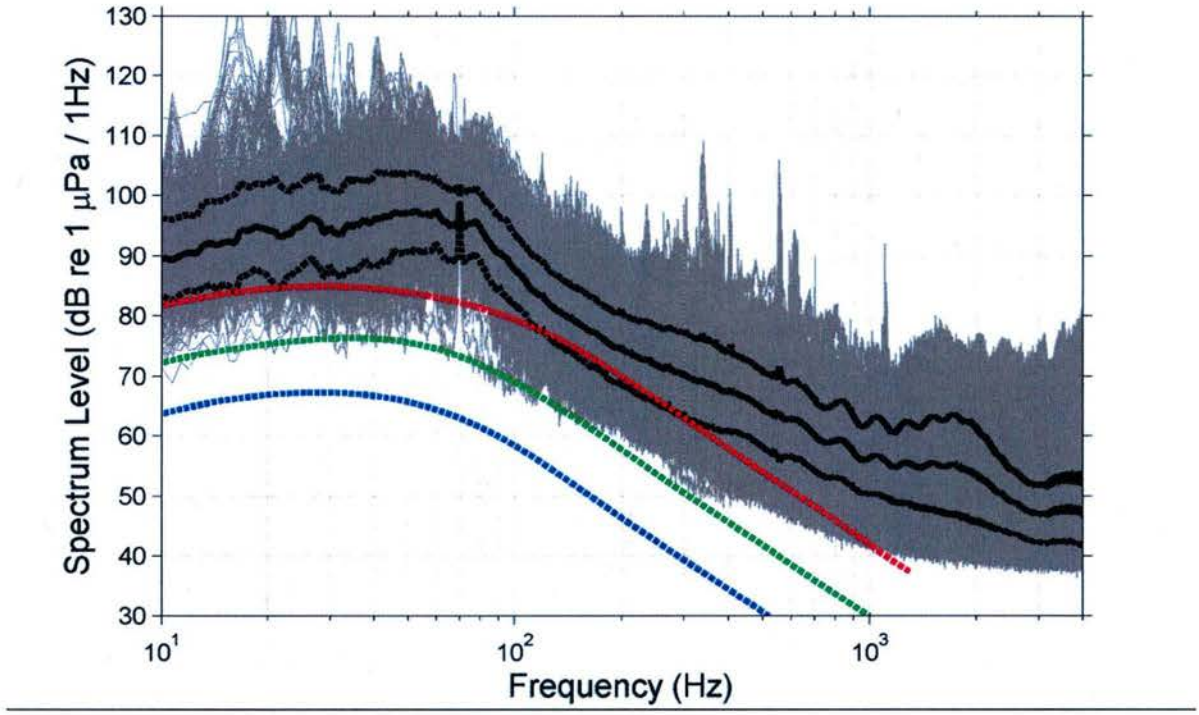

Figure 14. Ambient noise spectrum level during container ships passing by the acoustic engineering test site on the New England Mud Patch.

[The hydrophone deployment was 5.5 days, and the noise spectrum level curves within a 2 hour time window around every closest approach point of the container to the hydrophone array are shown. Total 35 containers were detected acoustically, and the total analyzed time for the ambient noise was 65 hours long. The black lines denote the mean and one standard deviation curves. The color curves are the average levels of heavy, moderate and light shipping noise in deep ocean (11).]